Effects of Hydrogen and Syngas Addition on the Ignition of Iso-octane/Air Mixtures

BY

SUDHANSHU JAIN
M.S., University of Illinois at Chicago, Chicago, 2012

THESIS

Submitted as partial fulfillment of the requirements
for the degree of Master of Science in Mechanical Engineering
in the Graduate College of the
University of Illinois at Chicago, 2012

Chicago, Illinois

Defense Committee:

Dr. S.K. Aggarwal, Chair and Advisor
Dr. Kenneth Brezinsky
Dr. Rodica Baranescu

DEDICATION

This dissertation is dedicated to my family and my friends.

ACKNOWLEDGMENTS

I would like to begin this section by thanking my advisor, Professor S.K. Aggarwal, for all of the mentoring, instruction, and support that I received. I would also like to acknowledge my committee members Professor Kenneth Brezinky and Professor Rodica Baranescu, for agreeing to be part of my committee and willing to help me along the way.

I would also like to acknowledge all of the help I received from Dongru Li, Xu Han and all my colleagues at Flow and Combustion Simulation Laboratory.

TABLE OF CONTENTS

LIST OF FIGURES

LIST OF TABLES

SUMMARY

A reduced mechanism containing 38 species and 74 reactions has been developed to examine the ignition characteristics of iso-octane/H_2 and iso-octane/syngas blends at engine relevant conditions. The mechanism is validated using available the shock tube and RCM (Rapid Compression Machine) ignition data for iso-octane/air, H_2/air and syngas/air mixtures. Further validation is performed by comparing its predictions with those using the LLNL (Lawrence Livermore National Laboratory) detailed mechanism with 874 species and 3796 reactions for iso-octane, Conaire mechanism with 10 species and 21 reactions for H_2, and Davis mechanism consisting of 14 species and 38 reactions for syngas. Both LLNL and our reduced Mechanism is used to investigate the effect of H_2 and syngas on the ignition of iso-octane/air mixtures in a closed homogenous reactor at temperatures between 700-1400K, equivalence ratios between 0.5-2.0, and pressure of 55 atm. For both mechanisms, the effect of H_2 is relatively small for blends containing less than 50% H_2 by volume, but becomes increasingly significant for higher H_2 fractions. The addition of H_2 increases ignition delay at low temperatures (T<900K), and decreases it at high temperatures (T>1000K). For H_2 fractions above 80%, the ignition process is influenced more strongly by the H_2 oxidation chemistry, and does not exhibit the NTC behavior.

The CO addition seems to have a negligible effect on the ignition of iC_8H_{18}/air mixtures, except at low temperatures (T<900K) and for blends containing more than 90% CO by volume. Thus the ignition behavior of iC_8H_{18}/syngas blends is essentially determined by the iC_8H_{18} and H_2 oxidation chemistries.

The reduced mechanism is then used to perform sensitivity and reaction path analysis to provide further insight into the ignition behavior of blends.

1. Introduction

1.1 Background

Ignition delay time is an important parameter in the combustor design of most engines, including compression ignition engines, gas turbines, and advanced combustor concepts designed for low NOx emissions. Few key emerging technologies, such as one based on homogeneous charge compression ignition concept (HCCI), largely depends on Ignition delay time of the fuel. When fuel and oxidizer mixture are allowed to react a host of intermediate radical species are produced and consumed. Oxidation of fuel to final products is not a global reaction i.e. fuel being converted to product in a single step reaction, instead many elementary reactions occur simultaneously to produce and consume a host of intermediate species eventually forming the product. Set of these elementary chemical reactions constitute chemical mechanism. As the elementary reaction progress, heat is released and temperature of the system increases. The increase in the temperature further accelerates the formation and consumption of radical species and temperature starts rising rapidly. The time lag between the introduction of fuel and oxidizer mixture and rapid rise of temperature and pressure is termed as Ignition delay. Ignition delay of fuel/air mixtures depends on many factors such as pressure, temperature composition of fuel/air mixture, chemical kinetic etc. For predicting ignition delay knowledge of chemical kinetics is very important.

Ignition delay is of most importance in internal combustion engines. In SI engines the knocking behavior is caused due to auto ignition of a portion of fuel/air/residual gas mixture ahead of the advancing flame. The combustion process in a CI engine is significantly affected by the ignition delay period of fuel. In CI engine ignition delay is the period between the start of

fuel injection into the combustion chamber and start of combustion and also depends on other physical phenomenon such as fuel vaporization and mixing. Unlike CI engines, auto ignition in Gas turbine engines is undesirable as ignition of the reactive mixture upstream of the combustion chamber can cause instabilities in the flame. Consequently, the ignition behavior of all practical fuels has been studied for a long time.

1.2 Motivation

Environmental concerns and desire to reduce dependency on fossil fuels have accelerated efforts to develop renewable and cleaner fuels for transportation and power generation. In this context, hydrogen (H_2) and syngas (primarily a mixture of H_2 and CO) are considered as a promising option for supplementing the use of conventional hydrocarbon fuels. Both H_2 and syngas fuels can be produced from a variety of renewable resources [1,2] and thus offer a virtually limitless supply.

The H_2 addition significantly extends the flammability limits and enhances the ignition and extinction characteristics of HC flames, with important consequences for. For instance, the enhanced ignitability due to H_2 addition can be used to improve the ignition performance of HCCI engines. The use of such blends is also well suited for spark–ignition (SI) engines, since a blend can be introduced through port injection or direct injection.

Hydrogen has many desirable combustion characteristics including wider flammability limits and high burning velocities. The extended lean flammability limit offers significant advantages in reducing NOx and soot emissions from practical combustors, either by operating at leaner conditions or using dilution, such as exhaust gas recirculation (EGR) in IC engines, in order to reduce flame temperatures. Similarly, the use of H_2 in gas turbine combustors can

improve their lean blowout and emissions characteristics. Hydrogen also has a high autoignition temperature, which coupled with its high flame speed and diffusivity, can provide good antiknock properties, improve charge homogeneity, and reduce cycle-to-cycle variation in spark–ignition (SI) engines. In spite of these advantages, the development of hydrogen-powered IC (H_2ICE) on a commercial scale has faced many challenges due to storage and safety issues associated with H_2, and its low energy content per unit volume. There are also technical challenges at high engine loads due to an increased propensity to preignite the hydrogen–air mixture and increased NOx production due to high temperatures [3, 4, 5].

A blended fuel strategy using a mixture of fossil fuel and H_2 (or fossil fuel and syngas) can address many of the above challenges. Moreover, such blends can be readily used within the existing infrastructure, and reduce greenhouse gas and other emissions associated with fossil fuels.

1.3 Literature Review

The idea of blending H_2 to enhance the properties of hydrocarbons is not new. Consequently, there have been numerous studies dealing with the ignition, combustion, and emission characteristics of H_2-hydrocarbon mixtures. Both fundamental and practical aspects of using such blends for transportation and power generation have been investigated. Fundamental studies have focused on CH_4/H_2 blends, and examined the effect of H_2 addition on flammability limits [6], laminar [7,8] and turbulent burning velocities [9], NOx emissions [10,11,12], flame propagation characteristics including flame speed-stretch interactions [13, 14], flame stability [15], and lean blowout limits [16]. There have also been engine studies on using various blends in compression ignition (CI) [17] and SI engines. Research dealing with SI engines has

considered blends of H_2 with methane [18, 19], natural gas [20, 21, 22, 23], CNG [24], gasoline [25,26, 27,28,29,30], biogas [31], methanol [32], and ethanol fuels [33]. An important result from these studies is that H_2 addition can generally provide noticeable improvement in engine performance in terms of combustion efficiency, increased burn rate, reduced cycle-to-cycle variations, and reduced CO, HC, and soot emissions. However, the actual effect depends on a number of factors, such as compression ratio, overall equivalence ratio, engine speed and load, spark timing, and amount of H_2 in the blend. This clearly underlines the need for further studies on engine optimization, and fundamental research on the effects of H_2 addition on the combustion and emission behavior of gasoline and surrogate fuels.

This paper reports a numerical investigation on the ignition of iso-octane/H_2 and iso-octane/syngas blends at engine relevant conditions. The study is motivated by the consideration of increasing the use of renewable fuels, such as H_2 and syngas, in IC engines, as discussed above. Moreover, the ignition characteristics of such blends are important for improving the performance of HCCI (Homogeneous Charge Compression Ignition) and PCCI (Premixed Charge Compression Ignition) engines. For instance, the addition of H_2 or syngas can provide an effective strategy for controlling the ignition event and expanding the operation range of HCCI combustion in terms of equivalence ratio and engine load. Such studies are also important from fundamental aspects, as previous research has mostly focused on the ignition of CH_4/H_2 blends. Zhang et al. [34] and Huang et al. [35] reported shock tube data, while Levinsky et al. [36] reported rapid compression machine (RCM) data on the ignition of CH_4/ H_2 blends for a range of pressures, temperatures, and blend compositions. The effect of H_2 was found to be negligible for blends containing less 60% H_2 by volume, while the ignition delay essentially resembled that of H_2 for blends containing more than 80% H_2. Aggarwal et al. [37] recently examined the effect of

H_2 addition on the ignition of n-heptane, which is considered a primary reference fuel and good surrogate for diesel. In this context, it is of interest to characterize the ignition behavior of effect of H_2 addition on the ignition behavior of iso-octane/H_2 blends, since iso-octane is also a primary reference fuel and good surrogate for gasoline. Similarly it is important to study the ignition behavior of iso-octane/syngas blends due to the potential of using syngas in dual fuel engines [38,39].

Thus our objective is to develop a reduced kinetic mechanism and examine the ignition behavior of iso-octane/H_2 and iso-octane/syngas blends at engine relevant conditions. The kinetic model was developed by incorporating important H_2 and syngas oxidation reactions into an iso-octane skeletal mechanism [40]. The combined mechanism was validated using the available experimental data for the ignition of iso-octane-air [41,42], H_2-air, and syngas-air mixtures [43,44]. Further validation was performed through comparison with predictions using the comprehensive mechanisms for the oxidation of iso-octane [45,46], H_2 [47,48], and syngas [49]. A numerical study was then conducted to characterize the ignition behavior of iso-octane/H_2 and iso-octane/syngas blends. Finally a sensitivity study was performed to identify the dominant reactions associated with the ignition of these blends, and to provide insight into the effects of H_2 and syngas on the ignition of iso-octane.

2. Physical Numerical Model

2.1 Problem Description

As discussed earlier when a fuel and oxidizer mixture is allowed to react, a number of intermediate species are produced and consumed through elementary reactions and heat is released. Consequently, concentration of intermediate species and system properties like temperature and pressure change with time. Change in concentration and temperature further changes the reaction rates of elementary reactions. As the detailed oxidation chemistry of practical fuels like n-heptane or iso-octane (which are surrogates for diesel and gasoline respectively) could involve few hundred intermediate species and elementary reactions, change in species concentration and system properties with time is calculated numerically.

2.2 Mathematical Model

The mathematical model is based on zero dimensional, closed homogenous, adiabatic reactor with constant volume conditions. The reactor system is isolated with no mass or energy flowing in or out of the system. Starting with first law of thermodynamics

$$Q - W = U \qquad 2.1$$

Here Q is heat loss, W is work done and U is internal energy. Assuming only work is Pdv work, W = 0 for a constant volume reactor. As mentioned above, the system is isolated and hence dQ/dt = 0. Differentiating once with respect to time, t, equation 2.1 is reduced to

$$\frac{dU}{dt} = 0 \qquad 2.2$$

Now U can be written as sum of internal energies of all the species, and assuming ideal gas behavior

$$U = \sum_i N_i \overline{u_i} \tag{2.3}$$

$$\frac{dU}{dt} = \sum_i N_i \frac{d\overline{u_i}}{dt} + \sum_i \overline{u_i} \frac{dN_i}{dt} = \sum_i N_i \overline{c_{vi}} \frac{dT}{dt} + \sum_i \overline{u_i} \frac{dN_i}{dt} = 0 \tag{2.4}$$

For an ideal gas

$$\overline{c_{vi}} = \overline{c_{pi}} - R_u \tag{2.5}$$

$$\overline{u_i} = \overline{h_i} - R_u T \tag{2.6}$$

$$\sum_i N_i (\overline{c_{pi}} - R_u) \frac{dT}{dt} + \sum_i (\overline{h_i} - R_u T) \frac{dN_i}{dt} = 0 \tag{2.7}$$

Since $N_i = V[X]_i$ and Volume is constant

$$\frac{dN_i}{dt} = V \frac{d[X]_i}{dt} \tag{2.8}$$

The equation 2.7 can be rewritten as

$$\frac{dT}{dt} = \frac{R_u T \sum_i \dot{\imath}_i - \sum_i \overline{h_i} \dot{\imath}_i}{\sum_i [[X_i](\overline{c_{pi}} - R_u)]} \tag{2.9}$$

Where

$$\bar{\imath}_i = \frac{d[X]_i}{dt} \tag{2.10}$$

N= number of moles

T = temperature

t = time
Q = rate of heat loss
R_u = universal gas constant
$\dot{\imath}$ = rate of production/ consumption of specie i
$\overline{h\imath}$ = molar enthalpy of specie i
[X] = concentration of specie i
$\overline{cp}$ = specific heat of specie i
The net production rate is given by

$$\dot{j} = \sum_{i=1} v_{ji}\, q_i \qquad 2.11$$

For the j[th] specie in i[th] reaction. Here

$$v_{ji} = (v''_{ji} - v_{ji}') \qquad 2.12$$

Where v''_{ji} and v_{ji}' are stoichiometric coefficients on the product and reactant side of the equation and q_i is the rate of progress variable which is defined as

$$q_i = k_{fi} \prod_{j=1}^{n} [X_j]^{v'_{ji}} - k_{ri} \prod_{j=1}^{n} [X_j]^{v''_{ji}} \qquad 2.13$$

Where kf and kr are the forward and reverse reaction rates of any reaction i. The expressions for reaction rates are written in three parameter functional form

$$k = A\, T^{b} \exp^{(-E_a/R_u T)} \qquad 2.14$$

Here, A is a constant called the pre exponential factor and E_a is the activation energy for the reaction. A, E_a, and b are all empirical parameters.

2.3 Numerical Simulation

Simulations were performed using the closed homogenous batch reactor model in CHEMKIN 10101. Note that the simulations under constant volume conditions have been shown to reproduce the shock tube and rapid compression machine (RCM) experiments reasonably well.

CHEMKIN uses an implicit time integration method to solve the transient stiff set of differential equations defined by equation 2.9 and 2.10

As discussed earlier the set of elementary reactions defining the oxidation of fuel is termed as Chemical Kinetic Mechanism. A mechanism could have several hundred reactions. All elementary reactions have all three empirical parameters (given by equation2.14), associated with them. This information is contained in a Chemical Kinetic Input file. A chemical input file must be provided by the user to CHEMKIN as it contains information about species, reactions associated reaction rate parameters. Appendix 1 shows the chemical kinetic mechanism for our reduced mechanism in CHEMKIN format with all three rate parameters.

Another input file provided to by the user is Thermodynamic Data file. The thermodynamic file contains the species name, its elemental composition, its electronic charge, and an indication of its phase (gas, liquid or solid). In addition, fourteen polynomial fitting coefficients are provided in the thermodynamic file that are used to calculate the specific heat, c_{pi}, specific enthalpy, h_i and specific entropy, s_i. The empirical relations used to calculate the these properties are given below

$$\frac{\bar{c_p}}{R_u} = a_1 + a_2T + a_3T^2 + a_4T^3 + a_5T^4 \qquad 2.15$$

$$\frac{\bar{h_\iota}}{R_u} = a_1 + \frac{a_2}{2}T + \frac{a_3}{3}T^2 + \frac{a_4}{4}T^3 + \frac{a_5}{5}T^4 + \frac{a_6}{T} \qquad 2.16$$

$$\frac{\bar{s_\iota}}{R_u} = a_1 lnT + a_2T + \frac{a_3}{2}T^2 + \frac{a_4}{3}T^3 + \frac{a_5}{4}T^4 + a_7 \qquad 2.17$$

Two set of constants a1-a7 are provided, for temperature 1000-5000 K and 300-1000 K making the total to 14 coefficients.

After providing the input files to Chemkin, we set the initial conditions namely initial pressure, P, temperature , T and initial mixture composition [X_i]for equations 9 and 10. Use has to provide the end time for the reaction. After the initial conditions are provided and thermodynamic properties are calculated CHEMKIN solves stiff set of differential equations to get the results.

The state of ignition was defined when the mixture temperature increases by 400 K with respect to initial temperature during simulations. Using other ignition criteria, such as one based on OH radical mole fraction, yielded essentially the same ignition delay time. Results are discussed in the next section. Figure 1 shows predicted temperature and OH time history for iso-octane mixture at an initial temperature 600 K (Figure 1 a) and 1000 K (Figure 1 b). Predicted time for temperature to increase by 400 K is also shown in Figure 1. As indicated in Figure 1 both the above mentioned criteria yield essentially the same ignition delay time.

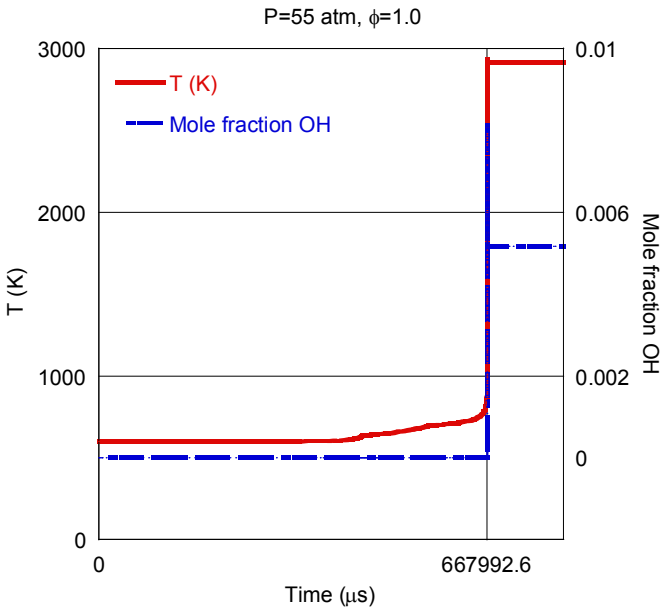

(a)

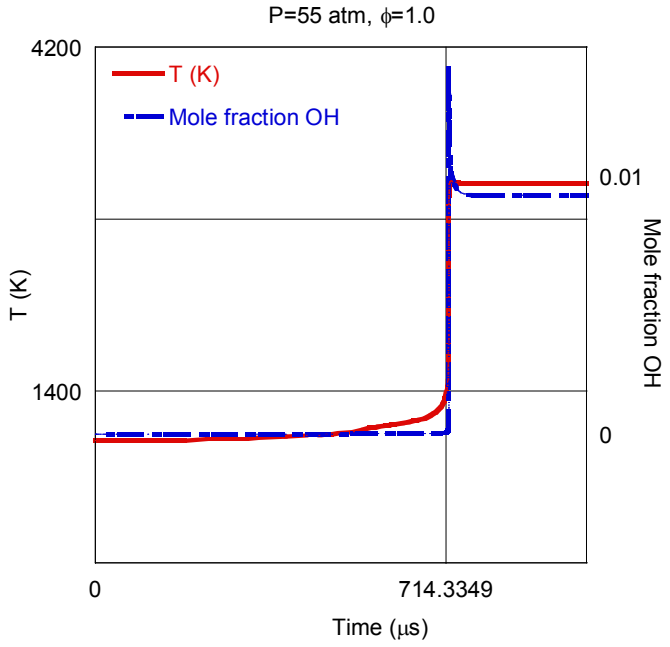

(b)

Figure 1: Predicted temperature and OH time histories for iso-octane/air mixtures at equivalence ratio ϕ= 0.1. P =55 atm and T 600 K (Fig a) and T =1000 K (Fig b). Predictions are based on our reduced mechanism.

3. Results and Discussion

3.1. Development of a Reduced Mechanism for Iso-octane/H_2/CO Blends

The starting point in the development of a reduced mechanism for iso-octane/H_2/CO blends was the Jia et al. skeletal mechanism [40], which has been optimized against ignition delay data under engine relevant conditions. We performed further validation of the mechanism using the detailed LLNL mechanism [50] and the shock tube and RCM ignition data for iso-octane/air mixtures. Figure 2 compares the predicted ignition delay times using these two mechanisms with the shock tube ignition data [41] at ϕ =0.5 (Figure 2 a) and 1.0 (Figure 2 b). Note that the experimental data has been normalized with respect to a pressure of 50 atm. As indicated in Figure 2, the Jia et al. mechanism exhibits reasonably good agreement with both the measurements and the predictions of the LLNL mechanism. In particular, it captures the NTC behavior as characterized by the drop in ignition delay as the initial temperature is reduced. Compared to the LLNL mechanism, the reduced mechanism indicates a slightly higher rolloff temperature and a more severe rolloff. Figure 3 presents the corresponding comparison with the RCM data [42] at ϕ=0.4. Again, there is good agreement between predictions and measurements, although both the mechanisms slightly underpredict ignition delays compared to experiments, especially at higher temperatures.

While the Jia et al. mechanism was able to reproduce the experimentally observed ignition behavior for iso-octane/air mixtures, it required modifications for predicting the ignition delays for H_2/air and syngas/air mixtures. Conaire et al. [47] mechanism and Davis et al. [49] mechanism were used to identify the most important reactions associated with the ignition of H_2/air and syngas/air mixtures, respectively. Sensitivity analysis was performed to identify most

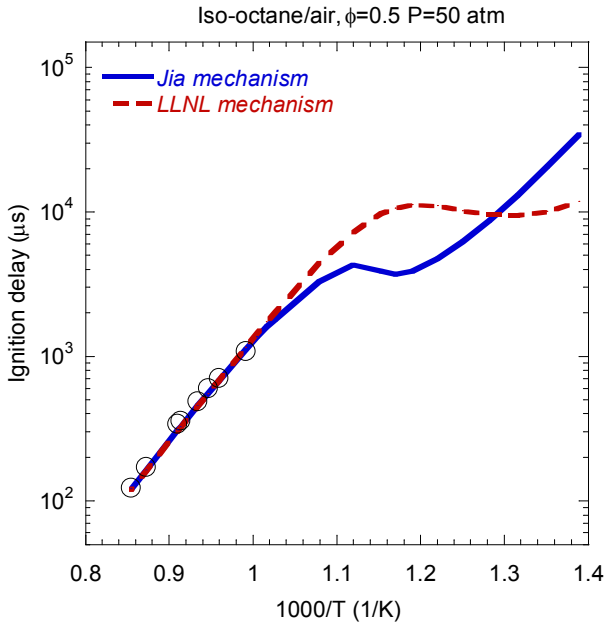

(a)

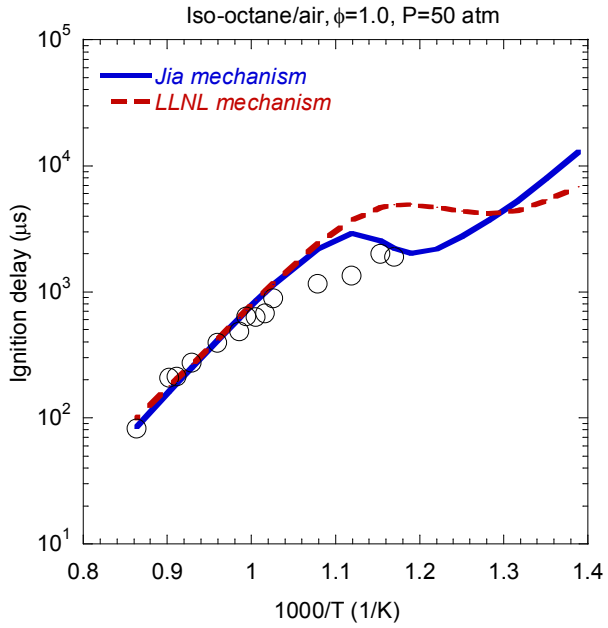

(b)

Figure 2: Predicted and measured ignition delay times for iso-octane/air mixtures at equivalence ratio ϕ = 0.5 (Fig1a) and ϕ =1.0 (Fig 1b). Predictions are based on Jia et al. [40] mechanism (solid line) and the detailed LLNL mechanism [50] (dashed line), while shock tube measurements (open circle), normalized to a pressure of 50 atm, are from Davidson et al. [41].

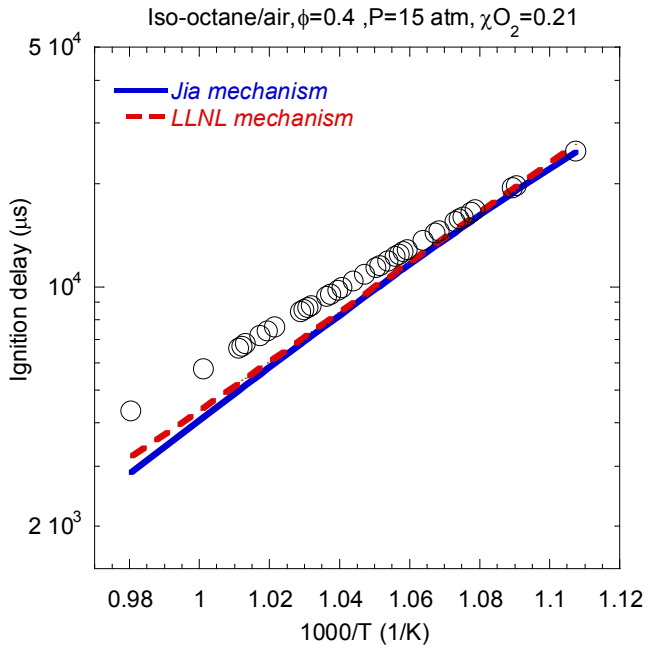

Figure 3: Predicted and measured ignition delay times for iso-octane/air mixtures. Predictions are based on Jia et al. [40] mechanism (solid line) and the detailed LLNL mechanism [50] (dashed line), and the normalized RCM ignition data is from Walton et al. [42].

important reactions regarding the ignition. The normalized sensitivity of a reaction to ignition delay is defined as

$$S = \frac{\partial \ln \tau}{\partial \ln k} = \frac{k}{\tau}\frac{\partial \tau}{\partial k} \qquad (3.1)$$

Here τ is the predicted ignition delay and k is the rate constant of reaction under consideration. The value of S was determined by calculating the change in ignition delay time after doubling the reaction rate constant K (equation 2.14). Then Eqn. (1) reduces to

$$S = \frac{(\tau(2k) - \tau(k))}{\tau(k)} \qquad (3.2)$$

Thus a negative value of S implies reduction in ignition delay as the reaction rate constant (k) is increased. Figure 4 shows the computed values of S for the most important reactions associated with the ignition of H_2/air mixtures at two different pressures and a temperature of 900 K. Note

that both the forward and reverse reaction rates were doubled to calculate the normalized sensitivity coefficient, S. Among the key reactions identified above, the following three reactions were added to the Jia et al. mechanism.

$$O+H_2 = H+OH \quad \text{(R70)}$$

$$HO_2+H = H_2+O_2 \quad \text{(R71)}$$

$$H_2O_2+H = H_2+HO_2 \quad \text{(R72)}$$

Other reactions shown in Figure 4 were already present in the Jia et al. mechanism. As noted earlier, this mechanism contains 69 elementary reactions and the three reactions added are numbered after 69. These three reactions are colored red in Figure 4. Reactions R70 and R71 are the important initiation reactions for H_2 oxidation. The reverse reaction of R71 is necessary to initiate the reaction between H_2 and O_2 as it is only reaction involving molecular oxygen and hydrogen. Due absence of R 71 in mechanism of Jia et al. [40]there was no activity in simulation when initial fuel mixture was pure H_2. Another key reaction is R72, which becomes more active in the reverse direction at higher temperature, and enhances ignition through the production of H radicals. The sensitivity analysis performed at other temperature and equivalence ratio values identified the same key reactions as indicated in Figure 4.

A similar sensitivity analysis was performed for the ignition of syngas/air mixtures using the Davis mechanism [49]. Figure 5 shows the normalized sensitivity coefficients with respect to the most important reactions for the ignition of 50/50 H_2/CO (by volume) blend. Other conditions are the same as those in Figure 4 with T = 900 K and ϕ=1.0. As indicated in Figure 4 and Figure 5, the key reactions pertaining to H_2 oxidation are the same in the two mechanisms. Among the reactions shown in Figure 5, the following two reactions pertaining to CO oxidation (shown in red color) were added to the Jia mechanism:

$$CO+O_2 = CO_2+O \qquad (R73)$$

$$CO+HO_2 = CO_2+OH \qquad (R74)$$

Both of these reactions supplement the reaction R28 in converting CO to CO_2. The sensitivity analysis at a higher temperature (1400 K) revealed two other important reactions for CO oxidation:

$$CO + OH = CO_2 + H \qquad (R28)$$

$$HCO + M = H + CO + M \qquad (R41)$$

However, these reactions were already present in the Jia mechanism. Thus our modified reduced mechanism contained 74 reactions (Appendix 1) with five additional reactions added to the Jia mechanism.

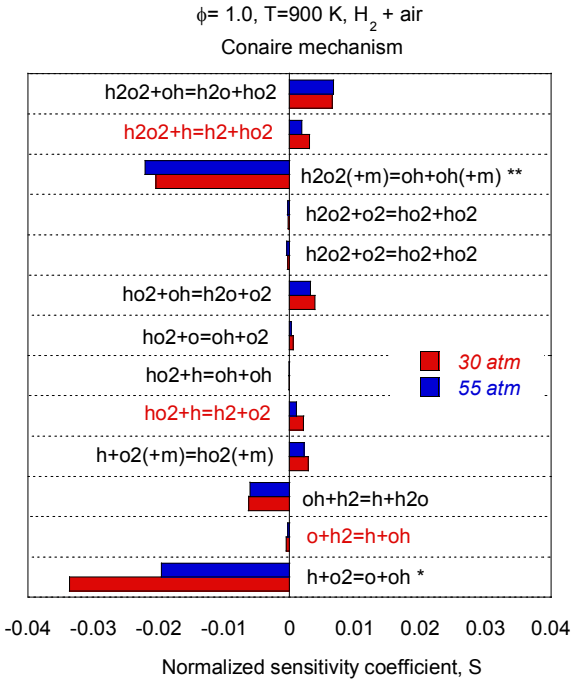

Figure 4: Normalized sensitivity coefficient, S for H_2/air mixtures at 30 atm and 55 atm. Other conditions are T= 900 K and ϕ=1.0. Simulations are based on the Conaire mechanism [47].* Plotted to 1/10th scale. ** Plotted to 1/2 scale.

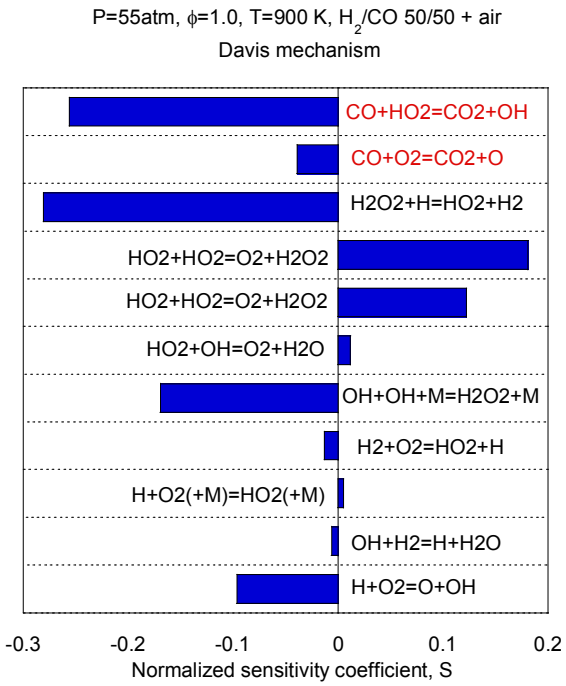

Figure 5: Normalized sensitivity coefficient (S) for syngas/air mixture with 50/50 H_2/CO blend at 55 atm, T= 900 K and ϕ=1.0. Simulations are based on the Davis mechanism [49].

3.2. Validation of the Reduced Mechanism

The modified reduced mechanism was first validated against the available shock tube ignition data for H_2/O_2/Argon mixtures. Figure 6 compares the predicted ignition delays for H_2/O_2/Argon mixtures with the shock tube [51]. The predictions using the Conaire mechanism [47] are also shown. As noted in the Figure 6, the shock tube ignition data is for high pressure and temperature. Comparison for two different pressure 33 atm and 64 atm is shown in Figure 6. There is good agreement between the predictions and measurements near temperatures 1200 K.

However, for temperatures higher temperatures both mechanisms slightly over predict the ignition delay time. Reaction sensitivity to ignition delay was calculated using equation 3.2 for important reaction regarding hydrogen oxidation using reduced mechanism as well as Conaire mechanism. Figure 7 shows the normalized sensitivity coefficients for H_2/air mixtures at

different temperatures using Conaire Mechanism (Figure 7 a) and our reduced mechanism (Figure 7 b). Note that in Figure 7a the reaction numbers provided in closed brackets are from Conaire et al. [47], and could be found online [52]. The corresponding reaction number in our reduced mechanism (Appendix 1) is also shown in Figure 7 a. As indicated in Figure 7 the normalized sensitivity coefficient, S for important reactions calculated using reduced mechanism were similar to the corresponding sensitivity coefficient calculated using Coanire mechanism.

The modified reduced mechanism was further validated against the available shock tube and RCM ignition data. Figure 8 and Figure 9 compare the predicted ignition delays for syngas/air mixtures with the shock tube [43] and RCM data [44], respectively. The predictions using the Davis mechanism [49] are also shown. As noted in these figures, the measured values are normalized with respect to a specific pressure. There is good agreement between the predictions

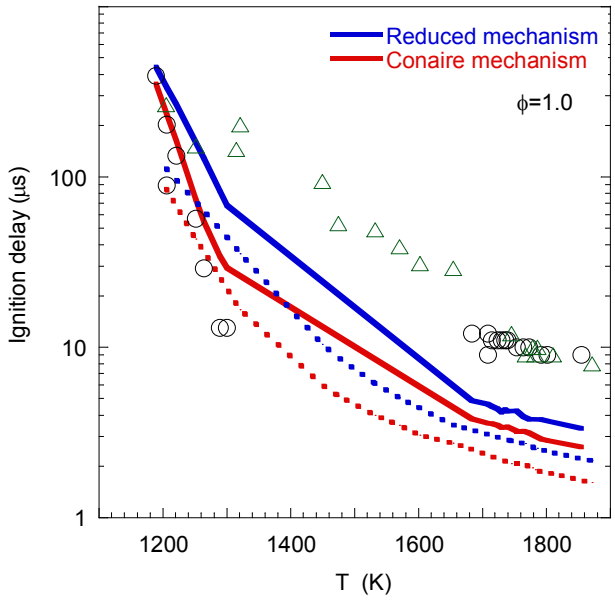

Figure 6: Predicted ignition delay times for H_2/O_2/Argon compared with shock tube ignition data [51] at pressure 33 atm (circles) and 64 atm (triangles). Prediction for P=33 atm (solid lines) and P=64 atm are based on our Modified mechanism (blue) and Conaire mechanism [47] red.

and measurements for temperatures above 1000 K. However, for temperatures below 1000 K, there are significant discrepancies between the predictions and experimental data. Similar discrepancies at low temperatures have been observed in previous studies [43,53]. In particular Dryer et al. [53] stated "ignition delay measurements in the mild ignition regime are strongly susceptible to perturbations and that model predictions of ignition delays that do not account for these perturbations can be significantly misleading".

Figure 8 and Figure 9 also indicate that our reduced mechanism under predicts the ignition delay compared to the Davis mechanism. Also, as shown in Figure 6 our reduced mechanism slightly over predicts ignition delay time compared to prediction of Conaire Mechanism. This can primarily be attributed to the different reaction rate constants for reaction R35 for dissociation of hydrogen peroxide:

$$H_2O_2 + M = OH + OH + M \qquad \text{(R35)}$$

R35 is a unimolecular reaction. Since the reactant of a unimolecular reaction must acquire sufficient energy before the reaction can take place, it requires intermolecular energy transfer through collision with another molecule. Consequently the unimolecular reaction is really second order in nature, exhibiting pseudo first-order behavior only under certain conditions. To demonstrate this, an arbitrary specie M is added in the reaction. The specific rate constant of unimolecular reaction is both pressure and temperature dependent. While rate constant is independent of pressure at high pressures it falls off at lower pressures. The most widely used representation of unimolecular reaction rate constant is Troe fall-off formula. Troe fall-off formula employs two set of reaction rate constants, one for high pressures (i.e when reaction rate constant, k is independent of pressure) namely k_∞, and one for fall off regime namely k_0. The rate constant is then defined as

$$k(T,p) = \left[\frac{1}{k0} + \frac{1}{k\infty}\right]^{-1} F(T,p)$$

Where, *F(T,p)* is called broadening factor. More details about *F(T,p)* can be found in Law[54] section 2.3.3. The rate constants for R35 used in our reduced mechanism were taken from the mechanism of Jia et al. [40], which is a skeletal mechanism for iso octane simulation optimized for HCCI engine simulations at high pressure. Consequently only one set of rate parameters were used in Jia mechamism. Table 1 shows the comparison of reaction rate constants for R35 for Conaire mechanism and our reduced mechanism.

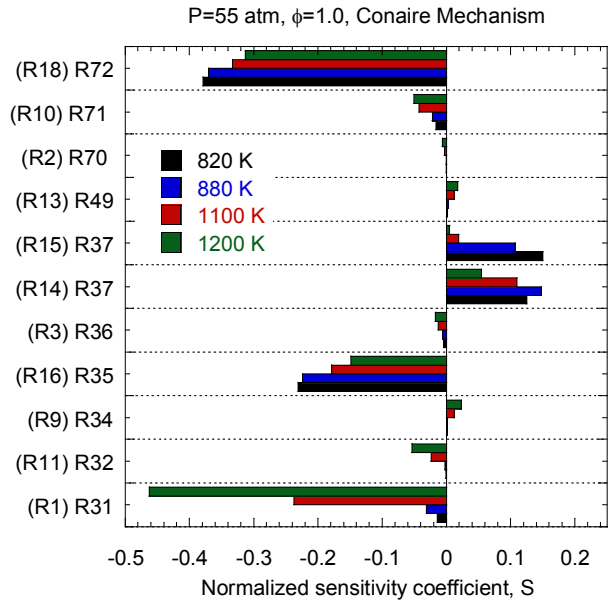

(a)

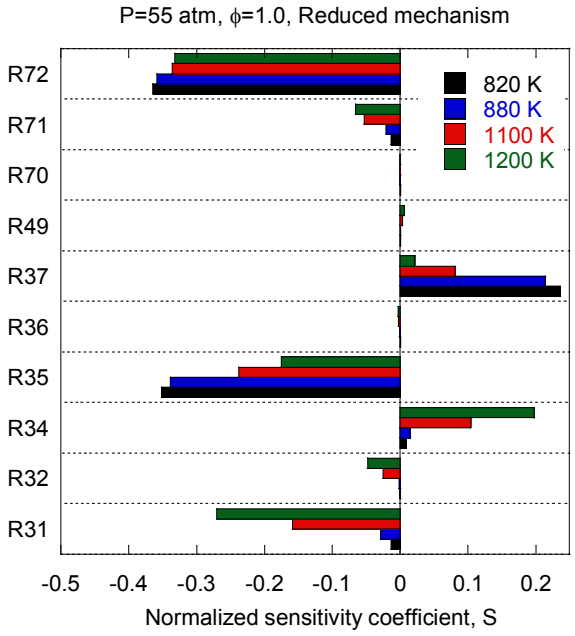

(b)

Figure 7: Normalized sensitivity coefficients, S for H_2/air mixtures using Conaire mechanism [47] (Fig a) and our reduced mechanism (Fig b) at four different temperatures. Bracketed reaction numbers in fig a are corresponding reactions numbers from Conaire mechanism.

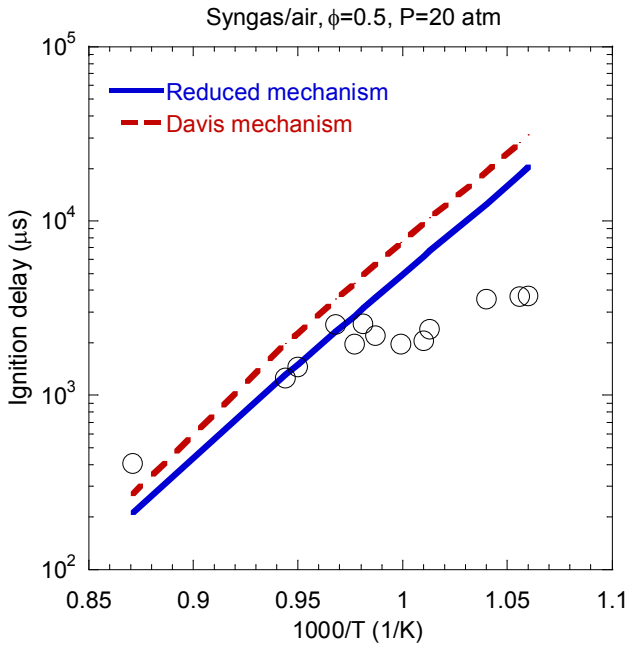

Figure 8: Predicted ignition delay for syngas compared with shock tube experimental data [43] (open circles). Predictions are based on our reduced mechanism (solid line) and Davis et al. [49] mechanism (dashed line). Experimental data has been normalized to 20 atm.

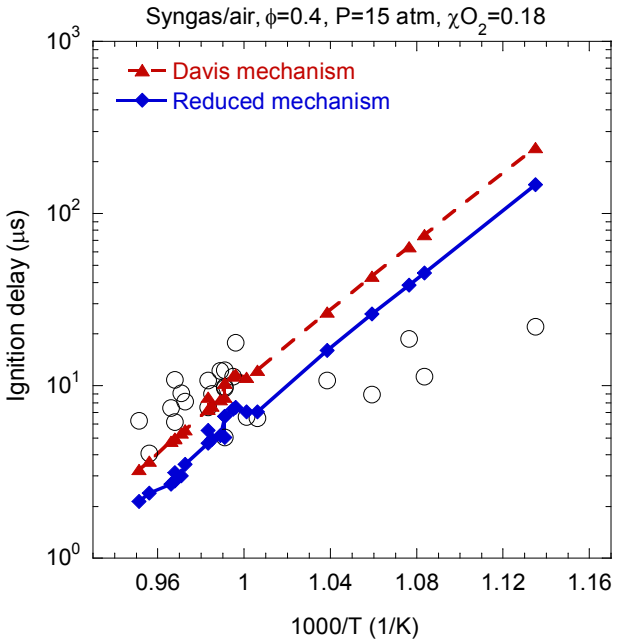

Figure 9: Predicted ignition delays for syngas/air mixtures compared with normalized RCM ignition data [44] (open circles). Predictions are based on our reduced mechanism (diamonds) and Davis et al. [49] mechanism (triangles). Experimental data is normalized to a pressure of 15 atm.

Table 1: Reaction rate constants for h2o2+m=oh+oh+m (R35) for Conaire mechanism and our reduced mechanism

	h_2o_2+m=oh+oh+m (R35)	A(mole-cm-sec-K)	b	Ea (cal/mole)
Reduced Mechanism	k	1.00 10E17	0	45500
h_2o Enhanced by	21.0			
co_2 Enhanced by	5.0			
h_2 Enhanced by	3.3			
co Enhanced by	2.0			
Conaire Mechanism[47]	High pressure, k_∞	2.95 10E14	0.00	48430
	Low Pressure, k_0	1.20 10E17	0.00	45500
h_2 Enhanced by	2.5			
h_2o Enhanced by	12.0			
ar Enhanced by	0.64			

It can be clearly seen that the rate constants used for R 35 in reduced mechanism are very similar low pressure rate constants for corresponding reaction in Conaire mechanism. It is also important to note that one could easily improve the agreement for the ignition of H_2-air mixtures by adjusting the above rate constants. However, this will affect the prediction of ignition delays for i-C_8H_{18}/syngas blends, since rate constants in our reduced mechanism have been optimized for have been optimized for these blends.

3.3. Analysis of the NTC Region

An important criterion for validating a mechanism especially for engine relevant conditions is that it should capture the NTC (negative temperature coefficient) chemistry

associated with the ignition of large hydrocarbon fuel species. In the present study, this aspect was examined through rate of production analysis and sensitivity analysis for our reduced mechanism, as discussed in the following.

Consistent with previous studies [45, 46], our analysis indicated that the fuel oxidation is initiated by H abstraction and production of alkyl radical through reaction R1

$$iC_8H_{18}+O_2=C_8H_{17}+HO_2 \qquad (R1)$$

Subsequently, the ignition chemistry is characterized by two competing routes depending upon the temperature. One route involves the production of alkylhydroperoxyradical through reactions R2 and R3, which then reacts with O_2 to form peroxy-alkylhydroperoxy radical. The latter species readily decomposes to form ketohydroperoxide through reaction R5, which then decomposes to form additional OH through reaction R6. This produces sufficient OH radical pool to accelerate the exothermic reactions and the ignition process, as indicated by reaction R7 that produces alkyl radical to feed into the below chain (R2–R7).

$$C_8H_{17}+O_2=C_8H_{17}O_2 \qquad (R2)$$

$$C_8H_{17}OO=C_8H_{16}OOH \qquad (R3)$$

$$C_8H_{16}OOH+O_2=OOC_8H_{16}OOH \qquad (R4)$$

$$OOC_8H_{16}OOH=OC_8H_{15}OOH+OH \qquad (R5)$$

$$OC_8H_{15}OOH=OC_8H_{15}O+OH \qquad (R6)$$

$$iC_8H_{18}+OH=C_8H_{17}+H_2O \qquad (R7)$$

At temperatures in the NTC region, the competing reaction pathway through reaction R8 becomes more active. This has the effect of slowing down the ignition process, as it leads to the

formation of H_2O_2 through reaction R37, which is known to be metastable specie at temperatures corresponding to the NTC regime and lower.

$$C_8H_{17} + O_2 = C_8H_{16} + HO_2 \quad \text{(R8)}$$

$$HO_2 + HO_2 = H_2O_2 + O_2 \quad \text{(R37)}$$

The relative contribution of each of these two pathways is illustrated in Figure 10, which plots the rate of production (ROP) or the consumption rate of O_2 for reactions R2 and R8 at different temperatures. At T=700 K, the O_2 consumption rate due to R2 is greater than that due to R8, while at T=800 K, which is in NTC regime, the two rates become comparable. At still higher temperatures, T=900 K and 1000 K, the O_2 consumption rate due to R8 significantly exceeds that due to R2, indicating clearly the slowing down of the first reaction pathway represented by R2-R6. As the temperature is increased further, i.e. above the NTC regime, the reaction R35 becomes active producing significant amount of OH radicals and accelerating the ignition process.

$$H_2O_2 + M = OH + OH + M \quad \text{(R35)}$$

The relative importance of reactions R2 and R8 was further assessed by computing the normalized sensitivity coefficient using Eq. (2). Figure 11 shows the normalized sensitivity coefficients for reactions R2 and R8 at different initial temperatures. As expected, the sensitivity coefficients for R2 and R8 have negative and positive values, respectively. The sensitivity coefficient for R8 has its highest values in the NTC regime, i.e., between 800 to 900K. Moreover, its value far exceeds that of R2 in the NTC regime, indicating that R8 noticeably slows down the ignition process in this regime. Figure 12 presents the normalized sensitivity coefficients for reaction R35 and R37. For temperatures above 700K, both of these reactions promote ignition. As discussed earlier, R37 produces H_2O_2, which is metastable species at lower

temperatures, but becomes increasingly active at temperatures above 900 K, providing OH radicals through reaction R35 and accelerating the ignition process. This is clearly illustrated in Figure 12. In summary, the above results clearly illustrate the capability of the reduced mechanism to capture the dominant reaction pathways characterizing the ignition process in the NTC region.

The ability of our modified mechanism to predict the ignition behavior of i-C_8H_{18}/H_2 blends was further assessed by comparing its predictions with those using the Conaire [47] and LLNL mechanism [50] for the ignition of H_2/air mixtures. Note that the Conaire mechanism for H_2 oxidation has been extensively validated using a variety of targets. Results for the ignition of H_2/air mixture at □=1, p=55 atm are presented in Figure 13, and clearly demonstrate the ability of the reduced mechanism to capture the H_2 ignition chemistry under engine relevant conditions. Having validated our reduced mechanism against the ignition data for iso-octane/air, syngas/air, and H_2/air mixtures, results now focus on the effects of H_2 and syngas addition on the ignition behavior of iso-octane/air mixtures.

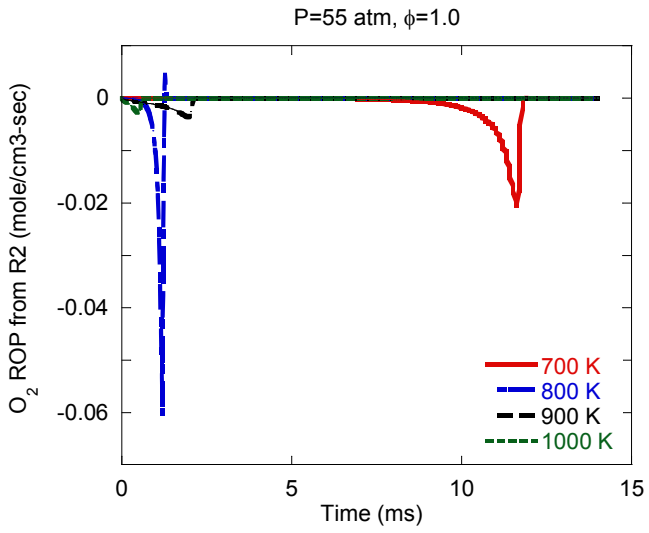

(a)

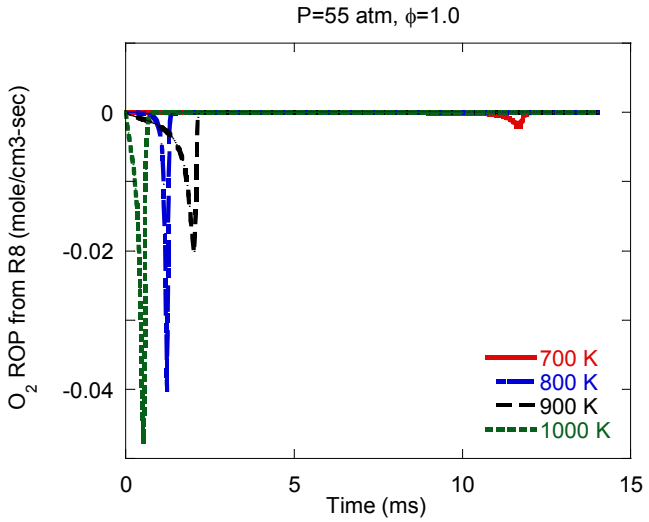

(b)

Figure 10: Rate of production of O2 due to reaction R2 (Fig a) and reaction R8 (Fig b) at different initial temperatures. Simulations are done using our reduced mechanism at pressure 55 atm and equivalence ratio ϕ=1.0.

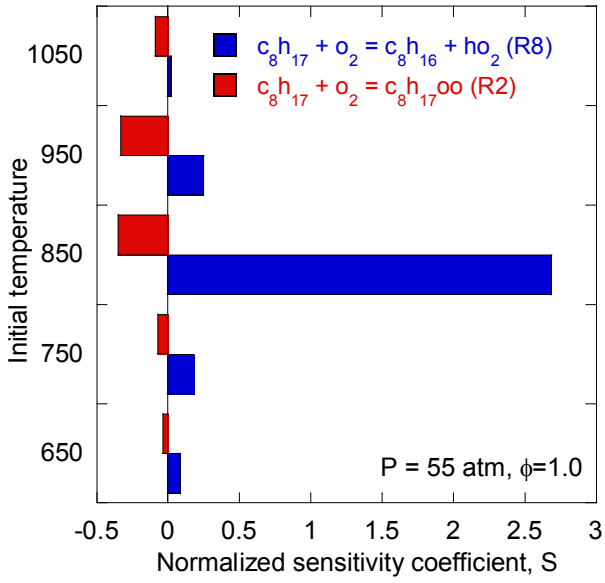

Figure 11: Normalized sensitivity coefficients for reactions R2 and R8 calculated at different initial temperatures using Eq. (3.2) for iso-octane/air mixture. Simulations are done using our reduced mechanism.

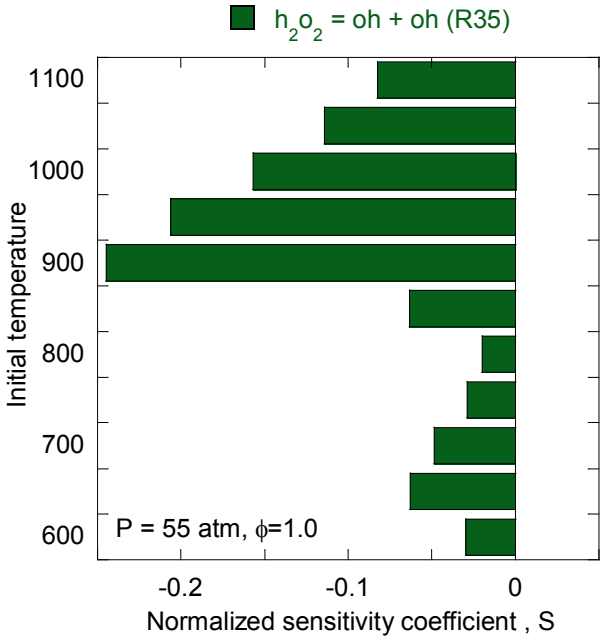

(a)

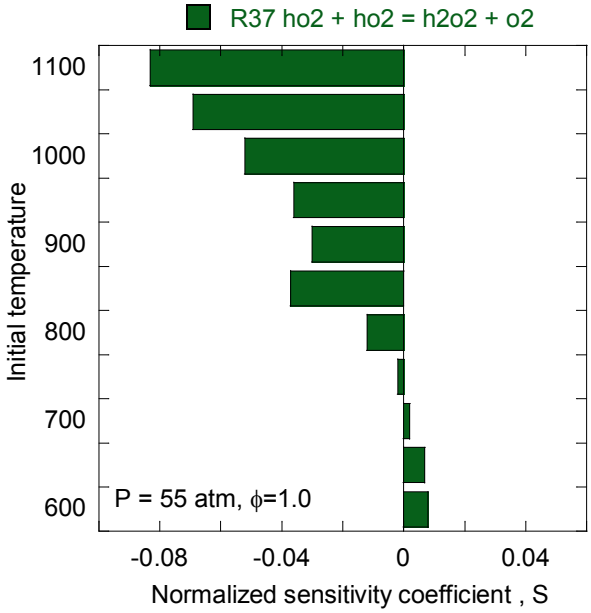

(b)

Figure 12: Normalized sensitivity coefficient calculated at different initial temperatures using Eq. (3.2) for iso-octane/air mixture for reactions R35 (Fig a) and R37 (Fig b) Simulations are based on our reduced mechanism.

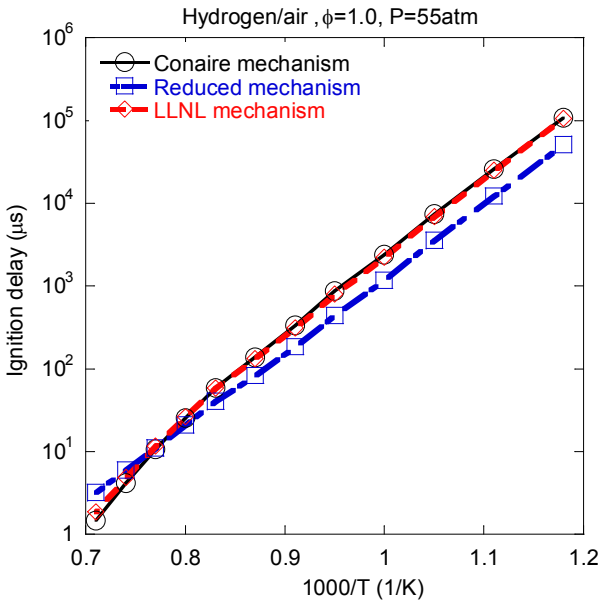

Figure 13: Predicted ignition delay times for H_2/air mixture using three different mechanisms. Predictions are based on our reduced mechanism (square) and Conaire et al. [47] mechanism (circle) and LLNL mechanism.

3.4. Effect of H_2 Addition on the Ignition of iC_8H_{18}/air Mixture

Figure 14 presents the effect of H_2 addition on the ignition of i-C_8H_{18}/air mixtures using our reduced mechanism and the LLNL mechanism. Results are shown in terms of the plot of ignition delay time as a function of initial temperature for six different iC_8H_{18}/H_2 blends at pressure p=55 atm, and different equivalence ratios. Results for the reduced mechanism are presented for ϕ=0.7, ϕ=1 and ϕ= 2, while those for the LLNL mechanism are for ϕ=1 (Figure 14 d). There is reasonably good agreement between the ignition delay predictions of the two mechanisms, although there are some quantitative differences. The effect of H_2 appears to be somewhat less pronounced with the LLNL mechanism, especially at lower temperatures (T < 900K). In general, for the both the mechanisms, the effect of H_2 addition is relatively small for H_2 fraction below 50% in the blend, but becomes increasingly significant for H_2 fraction above 50%. In particular, as the H_2 fraction exceeds 80%, the ignition behavior is strongly influenced by the H_2 oxidation chemistry. The overall effect of H_2 addition is to increase ignition delays at low temperatures (T < 900K), but increase it at high temperatures (T > 1000K). Further, for H_2 fraction exceeding 80%, the ignition delay plots do not exhibit the NTC behavior. Another interesting way to interpret the above results (Figure 14) is that the presence of a relatively small amount of i-C_8H_{18} (a low cetane number fuel) can significantly enhance the ignitability of H_2-air mixtures at temperatures below 1000K. This temperature range is important for HCCI and PCCI dual fuel engines.

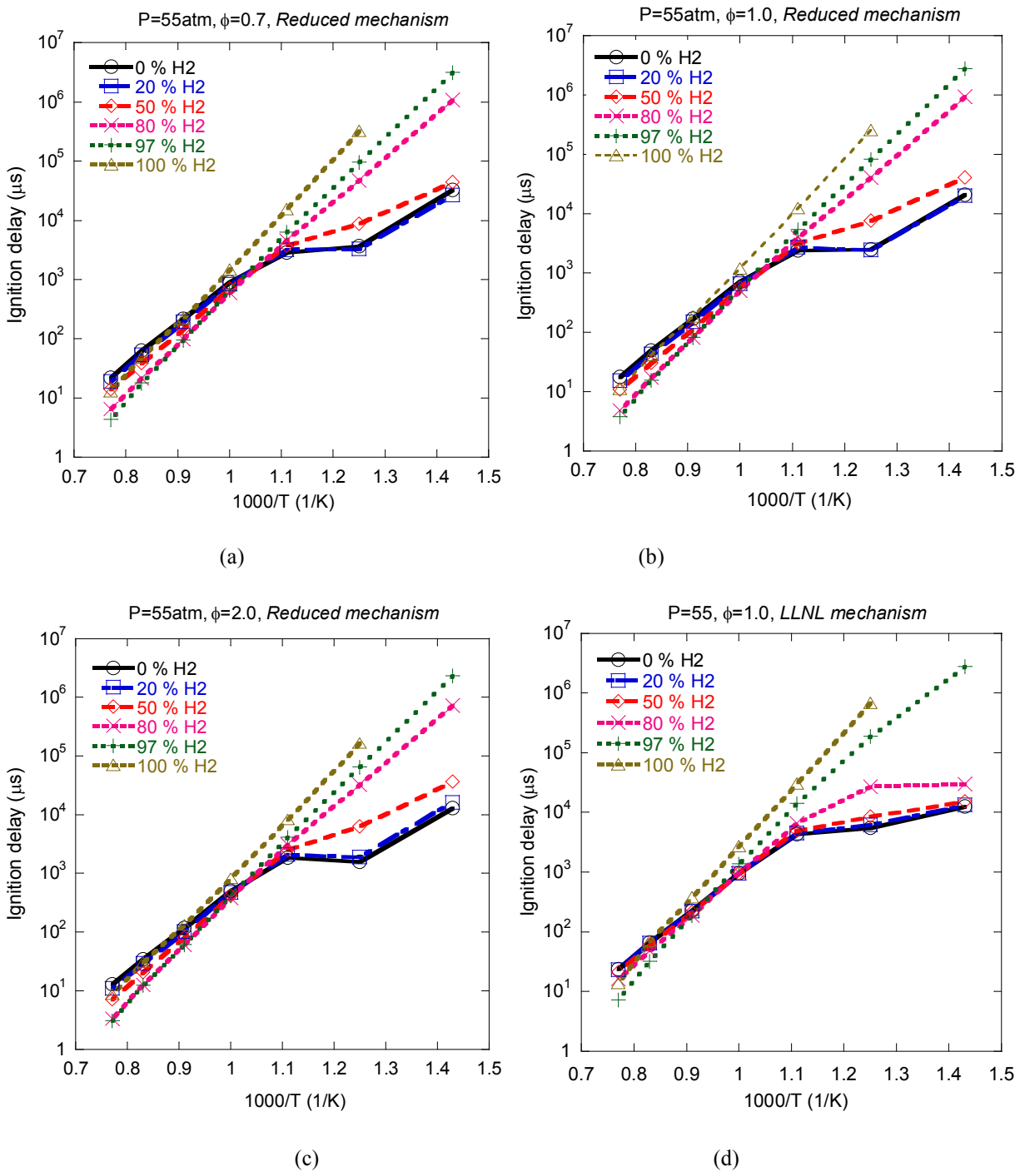

Figure 14: Predicted ignition delay times for iC8H18–H_2 blends with different amounts of H_2 (by volume) in the blend. Results for the reduced mechanism are shown for ϕ=0.7 (Fig. a), ϕ=1.0 (Fig. b), ϕ=2.0, (Fig. c), while those for the LLNL mechanism are for ϕ=1.0 (Fig. d). Pressure is 55 atm.

3.5. Effect of Syngas Addition on the Ignition of iC8H18/air Mixtures

Since syngas primarily contains H_2 and CO, the effect of syngas addition can be characterized in terms of the effect of CO on the ignition ofiC_8H_{18}/air mixtures. Figure 15 presents the ignition delay time times computed using the reduced mechanism (Figure 15 a) and LLNL mechanism (Figure 15 b) for different iC_8H_{18}/CO blends at p= 55 atm and ϕ=1.0. The addition of CO seems to have a negligible effect on the ignition of iC_8H_{18}/air mixtures, except at low temperatures (T< 900K) and for blends containing more than 90% CO by volume. Under latter conditions, the CO addition increases the ignition delay. However, it is difficult to envision using hydrocarbon-syngas blends with such large CO fractions, since the current research and development efforts are directed towards using hydrogen rich syngas through various carbon capture technologies. Figure 16 further shows the effect of CO in iC_8H_{18}/H_2/CO blends. The ratio of H_2 to iC_8H_{18} in Figure 16 is 3:1 by volume and is kept constant for all four blends while amount of CO has been increased. It can be clearly seen that CO has negligible effect on ignition of iC_8H_{18}/H_2/CO blends. Figure 17 shows syngas with 50/50 H_2/CO blended in iC_8H_{18}. As indicated in Figure 17, the ignition behavior of syngas/iso-octane blend is same as ignition behavior of H_2/iso-octane blend (Figure 14). Thus an important result here is that the ignition behavior of iC_8H_{18}/syngas blends is largely dominated by the oxidation chemistries of iC_8H_{18} and H_2.

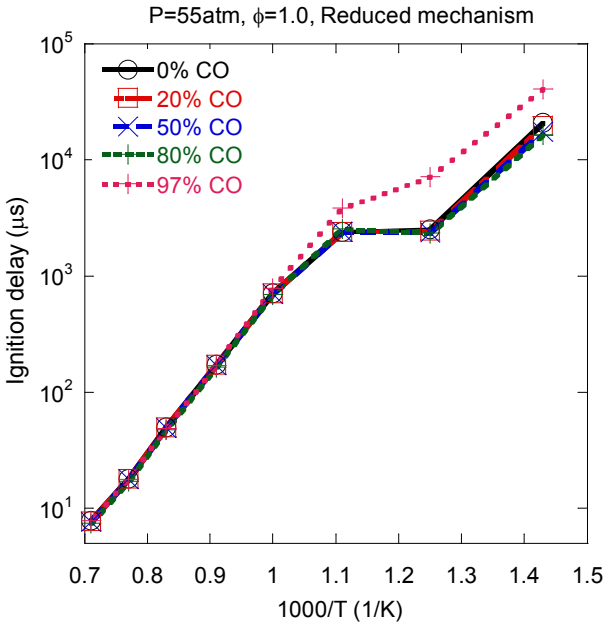

(a)

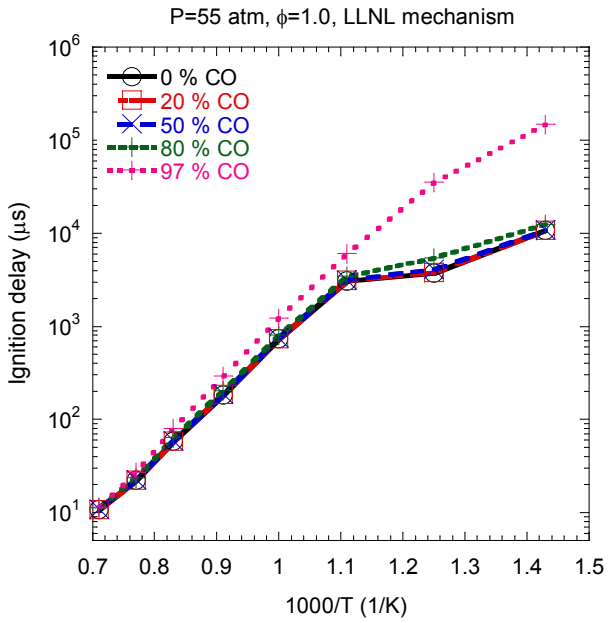

(b)

Figure 15: Predicted ignition delay time plotted for different iC_8H_{18}/CO blends at p= 55 atm and ϕ=1.0. Simulations were performed using the reduced mechanism (Fig. a) and the LLNL mechanism (Fig b).

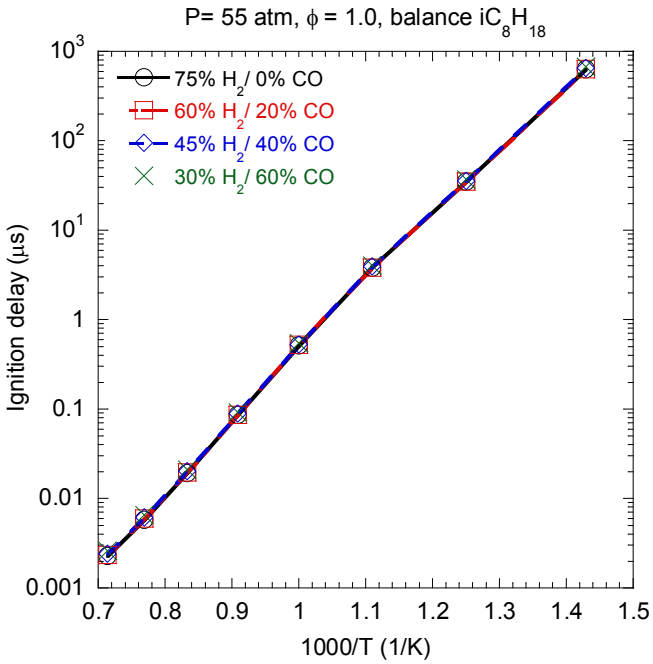

Figure 16: Predicted ignition delay time plotted for different $iC_8H_{18}/H_2/CO$ blends at P= 55 atm and ϕ=1.0. Simulations were are based on the reduced mechanism. Balance iC_8H_{18}.

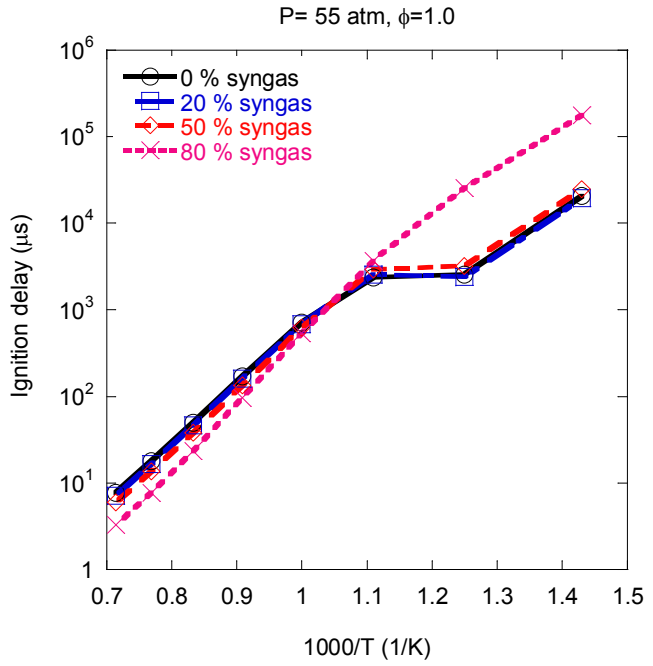

Figure 17: Predicted ignition delay time plotted for different iC_8H_{18}/syngas blends at P= 55 atm and ϕ=1.0. Simulations were are based on the reduced mechanism. Balance iC_8H_{18}.

3.6. Sensitivity and Reaction Path Analysis

The sensitivity and the reaction path analysis were performed in order to gain further insight into the effect of H_2 on the ignition of iC_8H_{18}/air mixtures. Figure 18 plots the normalized sensitivity coefficient with respect to various reactions for iC_8H_{18}/H_2 blends containing 0% and 80% H_2 by volume. Results for T=820K and 880K are presented to highlight the NTC region, while those for T=1100K are to characterize the high temperature ignition chemistry. The procedure for computing the sensitivity coefficients has been described in an earlier section. As discussed earlier, for the 0%H_2 case, the ignition chemistry in the NTC region is characterized by competition between the two oxidation routes represented by reactions R2 and R8, with R8 path dominating and thus increasing the ignition delay. This is clearly illustrated by the sensitivity coefficient plot in Figure 18 a. At higher temperatures (T=1100K), the important reactions affecting ignition include R1, R35, R37, and R49. Reactions R1, R35, R37 have been discussed in an earlier section, and, as expected, promote ignition. Reaction R49 ($HO_2 + OH = H_2O + O_2$) consumes radical species and thus increases the ignition delay.

For the 80%H_2 case, the presence of H_2 increases the ignition delay considerably in the NTC region, but decreases it in the high temperature region (Figure 14). The sensitivity results in Figure 18 indicate that the increase in ignition delay in the NTC region is primarily caused by reaction R36 ($H_2 + OH = H_2O + H$), which consumes OH radicals that are being produced through reactions R5 and R6, and feed the represented by reactions R2-R7, as part of the the iso-octane oxidation chemistry discussed earlier. Thus the depletion of OH radical pool due to reaction R36 slows down the ignition process in the NTC region. Moreover, the role of NTC chemistry becomes less important due to H_2 addition. The reduction of iso-octane fraction in the blend also make reactions R9 and R5, associated with the iso-octane oxidation, less important in the NTC

regime. At high temperatures (T=1100K), the effect of H_2 addition is to enhance the ignition process. This is due to the fact that for 80% H_2 in the blend, the ignition behavior is strongly influenced by the H_2 oxidation, as exemplified by reaction R31 ($O_2 + H = OH + O$) and R35, both of which decrease the ignition delay (Figure 18 b). In addition, Reactions R32 ($HO_2 + H = OH + OH$) and R36 ($H_2 + OH = H_2O + H$) become relatively important and reduce the ignition delay, but this effect is largely negated by reaction R34 ($H + O_2 + M = HO_2 + M$), which increases the ignition delay.

Another useful way to interpret the ignition of blends is that the addition of a relatively small amount iC_8H_{18} can significantly affect the ignition of H_2/air mixtures, especially. In particular, the presence of a low cetane number fuel, such as iC_8H_{18}, can noticeably enhance the ignitability of H_2 in the NTC region. Results summarizing this aspect are presented in Figure 19, which plots the normalized sensitivity coefficient with respect to various reactions for iC_8H_{18}/H_2 blends with 0%, 3%, and 80% iC_8H_{18} at T=820K and 1200K. As indicated in Figure 19 a, the reduction in ignition delay in the NTC region is primarily due to the opening up of the iC_8H_{18} oxidation route through reactions R1 and R7 discussed earlier. As the iC_8H_{18} mole fraction in the blend is increased, the reaction R8 becomes more important and, consequently, the ignition behavior is increasingly influenced by the NTC chemistry. At high temperatures (Figure 19 b), the increase in ignition delay due to iC_8H_{18} addition is mainly caused by the fact that iC_8H_{18} oxidation route through reactions R1 and R7 as well as the reaction R72, which promotes ignition, become less important.

Figure 20 presents the predicted reaction path diagrams for the ignition of iC_8H_{18}/H_2 blends with 0%H_2 (Figure 20 a) and 80%H_2 (Figure 20 b) at pressure=55 atm, initial temperature=850 K, ϕ=1.0, and time=0.975ms. Note that the ignition time for these cases were 1.82ms and 12.025ms,

respectively. The % with each arrow indicates the percentage of a species being consumed by a given reaction; for example, in Figure 20 a, 98.9% of iC_8H_{18} is being consumed by reaction R7 to produce the alkyl radical, while only 40.4% of OH is consumed in this reaction. For both cases, the iso-octane oxidation starts with production of alkyl radical by H abstraction through reaction R1, as discussed earlier with respect to the NTC behavior. Note, however, that this reaction is not shown in Figure 20 a for the 0%H_2 case, but indicated in Figure 20 b for the 80%H_2 case, since it is only significant early during the ignition process. Later during the ignition process, is mostly consumed through R7. The subsequent fuel oxidation path then follows two competing routes, as discussed earlier. One involves the production of ketohydroperoxide, which decomposes to form OH, which then reacts with iC_8H_{18} to produce alkyl radical to feed into this route, while the second route involves the formation of C_8H_{16} and HO_2. Both of these routes are active in both the 0% and 80%H_2 cases, as shown in Figure 20 However, for the latter case, the presence of H_2 opens another path for the consumption of OH through reaction R36 (Figure 18 b), and this has the effect of slowing down the iC_8H_{18} oxidation through its reaction with OH and reducing the production of C_8H_{17}. For example, as indicated in Figure 20, 40.4 % of OH consumption is used to produce alkyl radical (C8H17) in the 0%H_2 case compared to only 16.2 % in the 80%H_2 case.

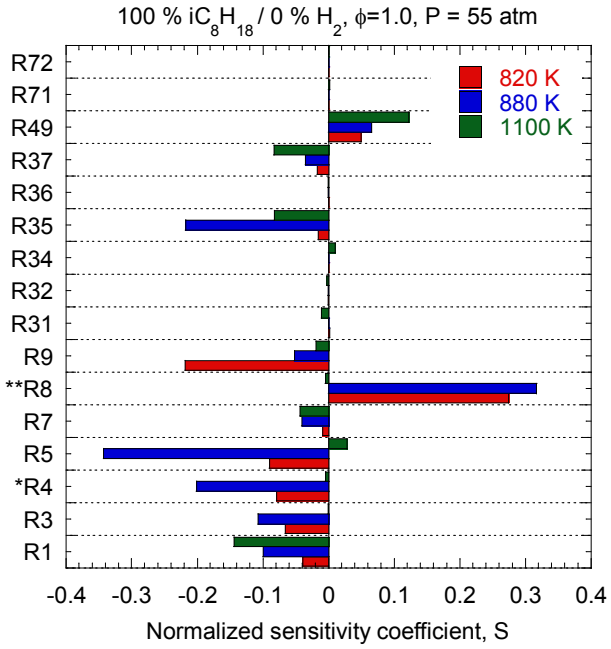

(a)

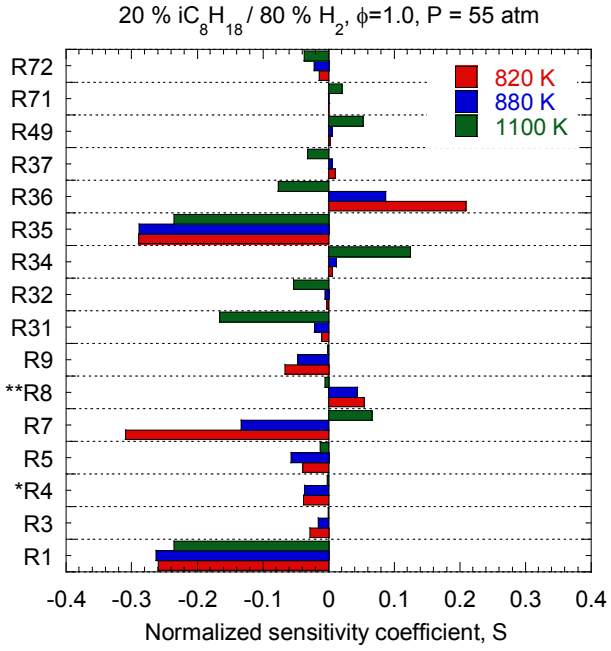

(b)

Figure 18: Normalized sensitivity coefficients calculated for 0% H_2 (Fig a) and 80% H_2 (Fig b) at three different temperatures. Simulations are based on our reduced mechanism. * Plotted to 1/2 scale. ** Plotted to 1/4 scale.

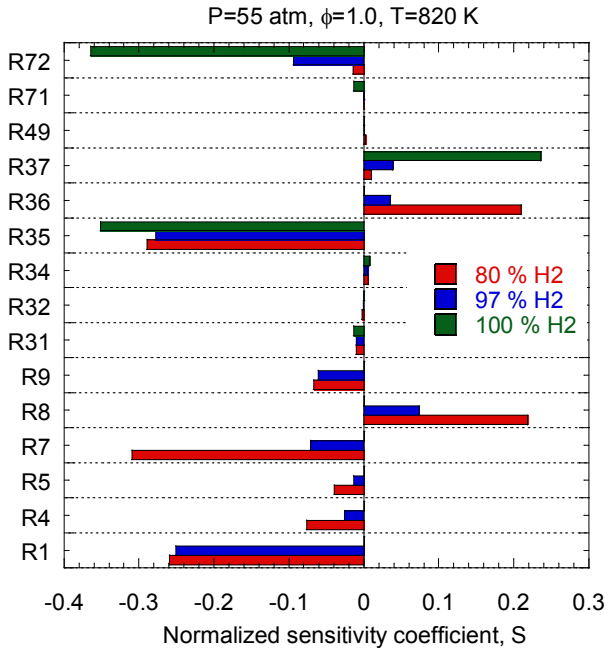

(a)

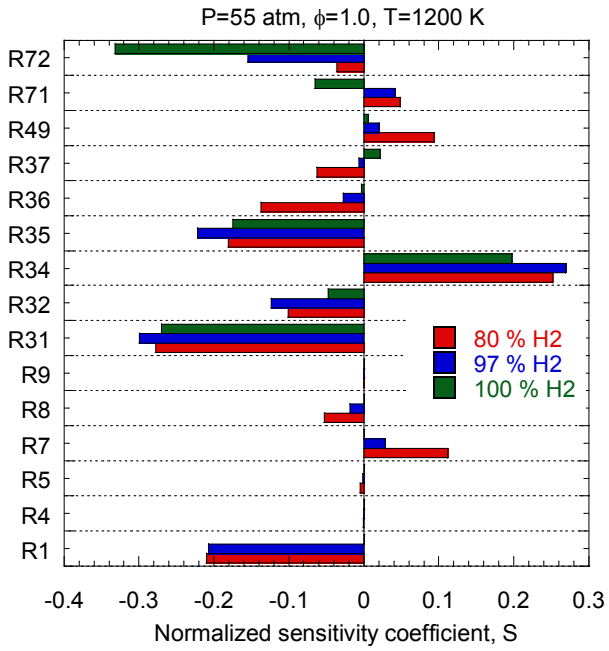

(b)

Figure 19: Normalized sensitivity coefficients calculated for 80% H_2, 97% H_2 and 100% H_2 in the iC8H18/H_2 at 820 K (a) and 1200 K (b). Simulations are based on our reduced mechanism.

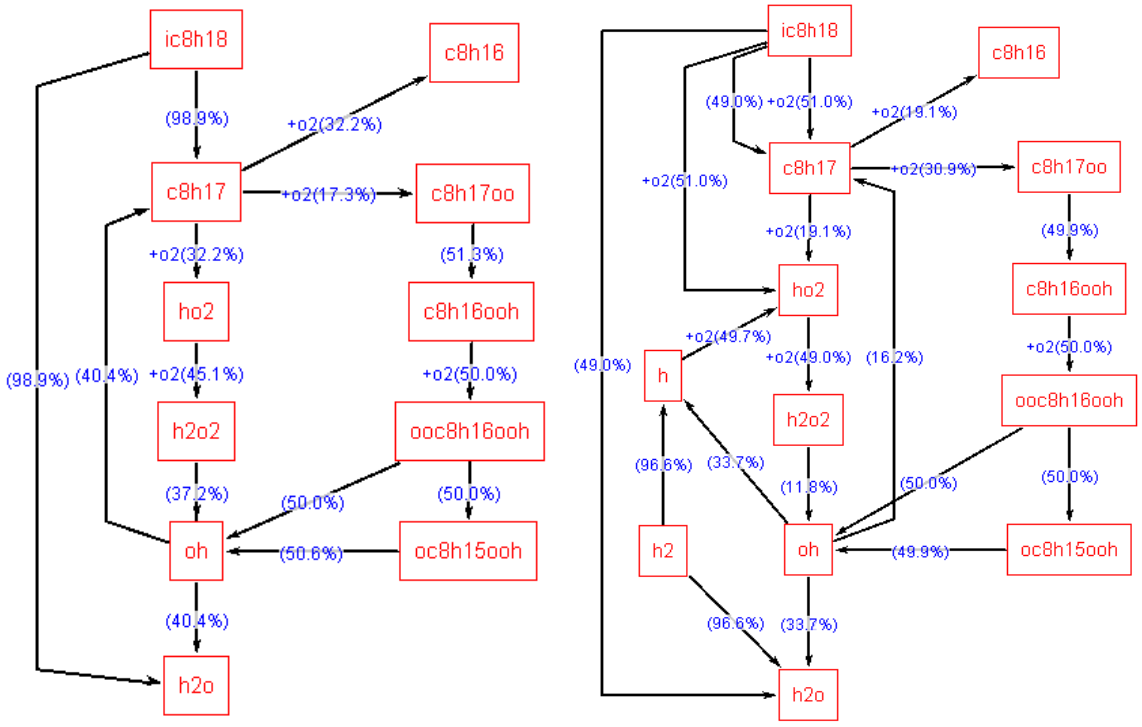

(a) **(b)**

Figure 20: Reaction pathway analysis for two iC_8H_{18}/H_2 blends with 0% H_2 (Fig a) and 80% H_2 (Fig b). Other conditions are p= 55 atm, T= 850 K, ϕ=1.0 and time=975 µs. Simulations are based on our reduced mechanism.

4. Conclusion

4.1 Summary

A reduced mechanism containing 38 species and 74 reactions has been developed to examine the ignition characteristics of iso-octane/H_2 and iso-octane/syngas blends at engine relevant conditions. The mechanism was validated using the shock tube and RCM ignition data for iso-octane/air, H_2/air and syngas/air mixtures. Further validation was performed by comparing its predictions with those using the LLNL detailed mechanism with 874 species and 3796 reactions for iso-octane, Conaire mechanism with 10 species and 21 reactions for H_2, and Davis mechanism consisting of 14 species and 38 reactions for syngas. The reduced mechanism was then used to characterize the effects of H_2 and syngas on the ignition of iso-octane/air mixtures in a closed homogenous reactor at temperatures between 700-1400K, equivalence ratios between 0.5-2.0, and pressure of 55 atm. The sensitivity and reaction path analysis were also performed to provide further insight into the ignition behavior of blends. Important observations are:

1. The reduced mechanism shows good agreement with shock tube and RCM measurements for the ignition of iso-octane/air, H_2/air and syngas/air mixtures. It also reproduces the experimentally observed NTC regime for iso-octane/air mixtures. However, there are significant discrepancies between its predictions and RCM data for syngas/air mixtures at lower temperatures ($T<1000$ K). Similar discrepancies have been observed by other researchers using the LLNL and the Davis mechanisms, and attributed to mixture nonhomogeneities present in the RCM experiments, but are not duplicated in simulations.
2. There is good agreement between the predictions of the reduced mechanism and the three detailed mechanisms for the ignition of iso-octane/air, H_2/air and syngas/air mixtures. The reduced mechanism also shows good agreement with the LLNL mechanism for the ignition

of iso-octane/H_2 and iso-octane/syngas blends. For both mechanisms, the effect of H_2 is relatively small for blends containing less than 50% H_2 by volume, but becomes increasingly significant for higher H_2 fractions. The addition of H_2 increases ignition delay at low temperatures (T<900K), and decreases it at high temperatures (T>1000K). For H_2 fractions above 80%, the ignition process is influenced more strongly by the H_2 oxidation chemistry, and does not exhibit the NTC behavior.

3. Another useful interpretation of the present results is that the addition of a relatively small amount of i-C_8H_{18} (a low cetane number fuel) can significantly enhance the ignitability of H_2-air mixtures at temperatures below 1000K. This temperature range is important for HCCI and PCCI dual fuel engines.
4. The CO addition seems to have a negligible effect on the ignition of iC_8H_{18}/air mixtures, except at low temperatures (T<900K) and for blends containing more than 90% CO by volume. Thus the ignition behavior of iC_8H_{18}/syngas blends is essentially determined by the iC_8H_{18} and H_2 oxidation chemistries
5. The sensitivity and reaction path analysis indicates that the iso-octane oxidation is initiated with the production of alkyl radical by H abstraction through reaction R1. Subsequently, for small amounts of H_2 in the blend, the ignition chemistry in the NTC region is characterized by a competition between two oxidation paths represented by reactions R2 and R8, with R8 path dominating, and increasing the ignition delay. As the amount of $_{H2}$ in the blend becomes significant, it opens up another path for the consumption of OH through reaction R36 (H_2 + OH H_2 H_2O + H). This has the effect of reducing the iC_8H_{18} oxidation through its reaction with OH, and thus slowing down the R2 path and increasing the ignition delay. However, at

temperatures T>1100K, the presence of H_2 decreases ignition delay primarily due to reactions R31 (O2 + H = OH + O) and R35 (H_2O2 + M = OH + OH + M).

4.2 Recommendation for future work

As discussed in validation section of results, ignition delay predictions based on our reduced mechanism slightly vary from Conaire mechanism and Davis mechanism. The variation is because pressure independent reaction rate constants have been used for unimolecular reactions. For predicting the hydrogen and syngas oxidation chemistry more accurately pressure dependent reaction rate constants have to be used for unimolecular reactions. As the the reaction rate constants used in reduced mechanism have been optimized for predicting ignition of iso-octane/air mixtures at high pressure, changing unimolecular reaction (R34 and R35) rate constants would affect predicted ignition delay time for iso-octane/air mixtures. Thus for accurately predicting ignition delay for iso-octane/air mixtures and hydrogen/syngas/air mixtures, reaction rate constants of decomposition reactions (R9-R12) have to be further modified.

The reduced mechanism developed in this study can further be validated against laminar flame speed and other experimental data associated with flames. The mechanism can be used in HCCI and dual fuel engine simulations for of iso-octane/ hydrogen/syngas blends as fuel where using a reduced mechanism can save considerable computational time. Similarly this mechanism can also be used in 2-D and 3-D flame simulation.

Appendix1: Reduced Mechanism Chemical Input File

	REACTIONS CONSIDERED	A (mole-cm-sec-K)	b	E (cal/mole)
1	ic8h18+o2=c8h17+ho2	1.00E+16	0	46000
	Reverse Arrhenius coefficients:	1.00E+12	0	0
2	c8h17+o2=c8h17oo	1.00E+12	0	0
	Reverse Arrhenius coefficients:	2.51E+13	0	27400
3	c8h17oo=c8h16ooh	1.14E+11	0	22400
	Reverse Arrhenius coefficients:	1.00E+11	0	11000
4	c8h16ooh+o2=ooc8h16ooh	3.16E+11	0	0
	Reverse Arrhenius coefficients:	2.51E+13	0	27400
5	ooc8h16ooh=>oc8h15ooh+oh	8.91E+10	0	17000
6	oc8h15ooh=>oc8h15o+oh	3.98E+15	0	43000
7	ic8h18+oh=>c8h17+h2o	1.00E+13	0	3000
8	c8h17+o2=c8h16+ho2	3.16E+11	0	6000
	Reverse Arrhenius coefficients:	3.16E+11	0	19500
9	oc8h15o+o2=>c2h3+2ch2o+c3h4+ch3+ho2	2.45E+13	0	32000
10	c8h17=>c4h8+c3h6+ch3	1.28E+12	0	49000
11	c8h16=>c4h8+c3h5+ch3	1.92E+12	0	48000
12	c4h8+o2=>c2h3+c2h4+ho2	2.00E+14	0	35900
13	c3h7=c2h4+ch3	9.60E+13	0	35900
14	c3h7=c3h6+h	1.25E+14	0	36900
15	c3h6+ch3=c3h5+ch4	9.00E+12	0	8480
16	c3h5+o2=c3h4+ho2	6.00E+11	0	10000
17	c3h4+oh=c2h3+ch2o	1.00E+12	0	0
18	c3h4+oh=c2h4+hco	1.00E+12	0	0
19	ch3+ho2=ch3o+oh	5.00E+13	0	0
20	ch3+oh=ch2+h2o	7.50E+06	2	5000
21	ch2+oh=ch2o+h	2.50E+13	0	0
22	ch2+o2=hco+oh	4.30E+10	0	-500
23	ch2+o2=co2+h2	6.90E+11	0	500
24	ch2+o2=co+h2o	2.00E+10	0	-1000
25	ch2+o2=ch2o+o	5.00E+13	0	9000
26	ch2+o2=co2+h+h	1.60E+12	0	1000
27	ch2+o2=co+oh+h	8.60E+10	0	-500
28	co+oh=co2+h	5.99E+07	1.3	5232.9
29	oh+ch3o=h2o+ch2o	5.00E+12	0	0
30	o+ch3o=oh+ch2o	1.00E+13	0	0
31	o+oh=o2+h	4.00E+14	-0.5	0
32	h+ho2=oh+oh	1.70E+14	0	875
33	oh+oh=o+h2o	6.00E+08	1.3	0
34	h+o2+m=ho2+m	3.60E+17	-0.7	0

		h2o Enhanced by	2.10E+01		
		co2 Enhanced by	5.00E+00		
		h2 Enhanced by	3.30E+00		
		co Enhanced by	2.00E+00		
35	h2o2+m=oh+oh+m		1.00E+17	0	45500
		h2o Enhanced by	2.10E+01		
		co2 Enhanced by	5.00E+00		
		h2 Enhanced by	3.30E+00		
		co Enhanced by	2.00E+00		
36	h2+oh=h2o+h		1.17E+09	1.3	3626
37	ho2+ho2=h2o2+o2		3.00E+12	0	0
38	ch2o+oh=hco+h2o		5.56E+10	1.1	-76.5
39	ch2o+ho2=hco+h2o2		3.00E+12	0	8000
40	hco+o2=ho2+co		3.30E+13	-0.4	0
41	hco+m=h+co+m		1.59E+18	0.9	56712.3
42	ch3+ch3o=ch4+ch2o		4.30E+14	0	0
43	c2h4+oh=ch2o+ch3		6.00E+13	0	960
44	c2h4+oh=c2h3+h2o		8.02E+13	0	5955
45	c2h3+o2=ch2o+hco		4.00E+12	0	-250
46	c2h3+hco=c2h4+co		6.03E+13	0	0
47	c2h5+o2=c2h4+ho2		2.00E+10	0	-2200
48	ch4+o2=ch3+ho2		7.90E+13	0	56000
49	oh+ho2=h2o+o2		7.50E+12	0	0
50	ch3+o2=ch2o+oh		3.80E+11	0	9000
51	ch4+h=ch3+h2		6.60E+08	1.6	10840
52	ch4+oh=ch3+h2o		1.60E+06	2.1	2460
53	ch4+o=ch3+oh		1.02E+09	1.5	8604
54	ch4+ho2=ch3+h2o2		9.00E+11	0	18700
55	ch4+ch2=ch3+ch3		4.00E+12	0	-570
56	c3h6=c2h3+ch3		3.15E+15	0	85500
57	n+no=n2+o		3.50E+13	0	330
58	n+o2=no+o		2.65E+12	0	6400
59	n+oh=no+h		7.33E+13	0	1120
60	n+co2=no+co		1.90E+11	0	3400
61	n2o+o=n2+o2		1.40E+12	0	10810
62	n2o+o=no+no		2.90E+13	0	23150
63	n2o+h=n2+oh		4.40E+14	0	18880
64	n2o+oh=n2+ho2		2.00E+12	0	21060
65	n2o+m=n2+o+m		1.30E+11	0	59620
66	no+ho2=no2+oh		2.11E+12	0	-480
67	no2+o=no+o2		3.90E+12	0	-240
68	no2+h=no+oh		1.32E+14	0	360

69	no+o+m=no2+m	1.06E+20	-1.4	0
70	o+h2=h+oh	5.08E+04	2.7	6292
	Reverse Arrhenius coefficients:	2.67E+04	2.6	4880
71	ho2+h=h2+o2	1.66E+13	0	823
	Reverse Arrhenius coefficients:	3.16E+12	0.3	55510
72	h2o2+h=h2+ho2	6.02E+13	0	7950
	Reverse Arrhenius coefficients:	1.04E+11	0.7	23950
73	co+o2=co2+o	1.12E+12	0	47700
74	co+ho2=co2+oh	3.01E+13	0	23000

References

1. Maschio G, Lucchesi A, Stoppato G. Production of syngas from biomass. Bioresource Technology. 1994:48:119–26.

2. Goransson K, Soderlind U, He J, Zhang W. Review of syngas production via biomass DFBGs. Renewable and Sustainable Energy Reviews 2011;15:482–92.

3. White CM, Steeper RR, Lutz AE. The hydrogen fueled internal combustion engine: a technical review. Int J Hydrogen Energy 2005;31:1292-1305.

4. Das LM. Exhaust emission characterization of hydrogen operated engine system: nature of pollutants and their control techniques. Int J Hydrogen Energy 1991;16:765–75.

5. Heffel JW. NOx emission reduction in a hydrogen fueled internal combustion engine at 3000 rpm using exhaust gas recirculation. Int J Hydrogen Energy 2003;28:1285–92.

6. Guo H, Smallwood GJ, Liu F, Ju Y, Gulder OL. The effect of hydrogen addition on flammability limit and NOx emission in ultra-lean counterflow CH4/air premixed flames. Proc. Combust Inst 2005; 30:303-11.

7. Yu G, Law CK, Wu CK. Laminar flame speeds of hydrocarbon + air mixtures with hydrogen addition. Combust Flame 1986;63:339-47.

8. Halter F, Chauveau C, Djebaıli-Chaumeix N, Gokalp I. Characterization of the effects of pressure and hydrogen concentration on laminar burning velocities of methane–hydrogen–air mixtures. Proc. Combust Inst 2005;30:201-8.

9. Shy SS, Chen YC, Yang CH, Liu CC, Huang CM. Effects of H2 or CO2 addition, equivalence ratio, and turbulent straining on turbulent burning velocities for lean premixed methane combustion Combust Flame 2008;153:510-24.

10. Naha S, Aggarwal SK. Fuel effects on NOx emissions in partially premixed flames. Combust Flame 2004; 39: 90-105.

11. Naha S, Briones AM, Aggarwal SK. Effect of fuel blends on pollutants emissions in flames. Combust Sci Technol 2005;177(1):183-220.

12. Guo H, Neill WS. A numerical study on the effect of hydrogen/reformate gas addition on flame temperature and NO formation in strained methane/air diffusion flames Combust Flame 2009;156: 477-83.

13. Halter F, Chauveau C, Djebaıli-Chaumeix N, Gokalp I.Characterization of the effects of pressure and hydrogenconcentration on laminar burning velocities of methan/hydrogen/air mixtures. Proc Combust Inst 2005; 30:201-8.

14. Briones AM, Aggarwal SK, Katta VR. Effects of H2 enrichmenton the propagation characteristics of CH4/air triple flames.Combust Flame 2008;153:367-83.

15. Tuncer O, Acharya S, Uhm JH. Dynamics, NOx and flashbackcharacteristics of confined premixed hydrogen-enrichedmethane flames. Int J Hydrogen Energy 2009;34:496-506.

16. Schefer RW. Hydrogen enrichment for improved lean flamestability. Int J Hydrogen Energy 2003;28:1131-41.

17. Shirk MG, McGuire TP, Neal GL, Haworth DC. Investigation of a hydrogen-assisted combustion system for a light-duty diesel vehicle. Int J Hydrogen Energy 2008;33:7237-44.

18. Bauer CG, Forest TW. Effect of hydrogen addition on the performance of methane-fueled vehicles. Part I: effect on SI engine performance, Int J Hydrogen Energy 2001;26:55-70.

19. Bauer CG, Forest TW. Effect of hydrogen addition on performance of methane-fueled vehicles. Part II: driving cycle simulation. Int J Hydrogen Energy 2001;26:71–90.

20. Nagalingam B, Duebel F, Schmillen K. Performance study using natural gas, hydrogen supplemented natural gas and hydrogen in AVL research engine, Int J Hydrogen Energy 1983;8(9):715–20.

21. Karim GA, Wierzba I, Al-Alousi Y. Methane-hydrogen mixtures as fuels, Int J Hydrogen Energy 1996;21(7):625–631.

22. Ma F, Wang Y, Liu H, Li Y, Wang J, Zhao S. Experimental study on thermal efficiency and emission characteristics of a lean burn hydrogen enriched natural gas engine. Int J Hydrogen Energy 2007;32:5067–75.

23. Ma F, Wang Y, Liu H, Li Y, Wang J, Ding S. Effects of hydrogen addition on cycle-by-cycle variations in a lean burn natural gas spark-ignition engine. Int J Hydrogen Energy 2008;33:823–31.

24. Das LM, Gulati R, Gupta PK. A comparative evaluation of the performance characteristics of a spark ignition engine using hydrogen and compressed natural gas as alternative fuels. Int J Hydrogen Energy 2000;25:783–93.

25. Sher E and Hacohen Y. Measurements and predictions of the fuel consumption and emission of a spark ignition engine fueled with hydrogen-enriched gasoline. J Power Energy 1989;203:155-159.

26. Changwei J, Shuofeng W. Effect of hydrogen addition on the idle performance of a spark ignited gasoline engine at stoichiometric condition. Int J Hydrogen Energy 2009;34:3546-56.

27. Andrea TD, Henshaw PF, Ting DSK. The addition of hydrogen to a gasoline –fuelled SI engine. Int J Hydrogen Energy 2004;29:1541–52.

28. Kahraman E, Ozcanl SC, Ozerdem B. An experimental study on performance and emission characteristics of a hydrogen fuelled spark ignition engine. Int J Hydrogen Energy 2007;32:2066–72.

29. Ma F, Wang Y, Liu H, Li Y, Wang J, Ding S. Effects of hydrogen addition on cycle-by-cycle variations in a lean burn natural gas spark-ignition engine. Int J Hydrogen Energy 2008;33:823–31.

30. Ji C,Wang S. Effect of hydrogen addition on combustion and emissions performance of a spark ignition gasoline engine at lean conditions. Int J Hydrogen Energy 2009;34:7823–34.

31. Porpatham E, Ramesh A, Nagalingam B. Effect of hydrogen addition on the performance of a biogas fuelled spark ignition engine. Int. J Hydrogen Energy 2007;32(12):2057–65.

32. Schafer F. An investigation of the addition of hydrogen to methanol on the operation of an unthrottled Otto engine, SAE Paper 810776, 1981.

33. Al-Baghdadi, MAS. Hydrogen–ethanol blending as an alternative fuel of spark ignition engines. Renewable Energy 2002; 28 (9):1471-1478.

34. Zhang Y, Huang Z, Wei L, Zhang J, Law CK. Experimental and modeling study on ignition delays of lean mixtures of methane, hydrogen, oxygen, and argon at elevated pressures. Combust Flame 2012;159:918-31.

35. Huang J, Bushe WK, Hill P G, Munshi SR. Shock initiated ignition in homogeneous methane-hydrogen-air mixtures at high pressure. Int. J. of Chemical Kinetics 2006;38(4):221-33.

36. Gersen S, Anikin NB, Mokhova AV, Levinsky HB. Ignition properties of methane/hydrogen mixtures in a rapid compression machine. Int J Hydrogen Energy 2008;33:1957-64.

37. Aggarwal SK, Awomolo O, Akber K. Ignition Characteristics of Heptane-Hydrogen and Heptane-Methane Fuel Blends at Elevated Pressures,Int J Hydrogen Energy 2011;36:15392-15402.

38. Boehman AL, Le Corre O. Combustion of Syngas in Internal Combustion Engines. Combust Sci and Tech 2008;180:1193–1206.

39. Azimov U, Tomita E, Kawahara N, Harada Y. Effect of syngas composition on combustion and exhaust emission characteristics in a pilot-ignited dual-fuel engine operated in PREMIER combustion mode. Int J Hydrogen Energy 2011;36:11985–96.

40. Jia M, Xie M. A chemical kinetics model of iso-octane oxidation for HCCI engines. Fuel 2006;85:2593-604.

41. Davidson DF, Gauthier BM, Hanson RK. Shock tube ignition measurements of iso-octane/air and toluene/air at high pressures. Proc. Combust Inst 2005;30:1175-82

42. Walton SM, He X, Zigler BT, Wooldridge MS, Atreya A. An experimental investigation of iso-octane ignition Phenomena. Combust Flame 2007;150:246–62.

43. Petersen EL, Kalitan DM, Barrett AB, Reehal SC, Mertens JD, Beerer DJ, et al. New syngas/air ignition data at lower temperature and elevated pressure and comparison to current kinetics models. Combust Flame 2007;149:244–47.

44. Walton SM, He X, Zigler BT, Wooldridge MS. An experimental investigation of the ignition properties of hydrogen and carbon monoxide mixtures for syngas turbine applications. Proc. Combust Inst 2007;31:3147–54.

45. Curran HJ, Gaffuri P, Pitz WJ, Westbrook CK. A Comprehensive Modeling Study of iso-octane oxidation. Combust Flame 2002;129:253-80.

46. Curran HJ, Pitz WJ, Westbrook CK, Callahan CV, Dryer FL. Oxidation of Automotive Primary Reference Fuels at Elevated Pressures. Proc. Combust Inst 1998;27:379-87.

47. Ó Conaire M, Curran HJ, Simmie JM, Pitz WJ, Charles K. Westbrook CK. A comprehensive modeling study of hydrogen oxidation. International Journal of Chemical Kinetics 2004;36:603-22.

48. Li J, Zhao Z, Kazakov A, Dryer FL. An Updated Comprehensive Kinetic Model of Hydrogen Combustion. International Journal of Chemical Kinetics 2004;36:566-75.

49. Davis SG, Joshi AV, Wang H, Egolfopoulos F. An optimized kinetic model of H2/CO combustion. Proc. Combust Inst 2005;30:1283-92.

50. https://www-pls.llnl.gov/?url=science_and_technology-chemistry-combustion-iso_octane_version_3

51. Petersen EL, Davidson DF, Rohrig M, Hanson RK.High-Pressure Shock-Tube Measurements of Ignition Times in Stoichiometric H2-O2-Ar Mixtures. International Symposium on Shock Waves. 1995;20:941-46.

52. https://www-pls.llnl.gov/data/docs/science_and_technology/chemistry/combustion/h2_v1b_mech.txt

53. Dryer FL, Chaos M. Ignition of syngas/air and hydrogen/air mixtures at low temperatures and high pressures: Experimental data interpretation and kinetic modeling implications. Combust Flame 2008;152:293–99.

54. Law CK. Combustion Physics. Cambridge University Press. 2006.

VITA

NAME	Sudhanshu Jain
EDUCATION	B.E., Mechanical Engineering, Bhopal University, India, 2008
EXPERIENCE	Research Aide, Flow and Combustion Simulation Laboratory, Mechanical and Industrial Engineering, University of Illinois at Chicago, 2011-2012 Teaching Assistant, Mechanical and Industrial Engineering, University of Illinois at Chicago, 2011-2012 Field Operations and Panel Engineer, Reliance Industries Limited, Bharuch, India, 2008-2010
PUBLICATIONS	"Effects of Hydrogen and Syngas Addition on the Ignition of Iso-octane/Air Mixtures" Submitted to International Journal of Hydrogen Energy